

# Insight into the Role of Guanidinium and Cesium in Triple Cation Lead Halide Perovskites

Susana Ramos-Terrón, José Francisco Illanes, Diego Bohoyo-Gil, Luis Camacho, and Gustavo de Miguel\*

The overall impact of the partial replacement (5–15%) of methylammonium (MA) in the MAPbI<sub>3</sub> perovskite by cesium or guanidinium (Gua) cations to fabricate thin films of triple cation Cs<sub>x</sub>Gua<sub>y</sub>MA<sub>1-x-y</sub>PbI<sub>3</sub> perovskites is studied.

The structural changes are investigated by using X-ray diffraction measurements revealing shrinkage or expansion of the unit cell upon Cs or Gua incorporation, respectively. The optoelectronic properties are characterized with photoluminescence (PL) time-resolved spectroscopy and the space charge limited current (SCLC) method. Shorter PL time constants are obtained for the samples with only Cs, while longer PL decays are measured for the perovskites containing additional Gua cation. The SCLC measurements reveal a larger density of trap states in the Cs<sub>x</sub>MA<sub>1-x</sub>PbI<sub>3</sub> perovskites compared to the MAPbI<sub>3</sub> material. The PSCs fabricated with the different mixed cation Cs<sub>x</sub>Gua<sub>y</sub>MA<sub>1-x-y</sub>PbI<sub>3</sub> perovskites reveal a good correlation with the measured optoelectronic properties. The power conversion efficiency (PCE) improves from an average value of 18.6% for the MAPbI<sub>3</sub> to a value of 20.0% for the Cs<sub>0.05</sub>Gua<sub>0.05</sub>MA<sub>0.90</sub>PbI<sub>3</sub> perovskite with a champion cell delivering 21.2%. On the opposite, the PCE decreases to a value of 17.3% for the double cation perovskite with Cs.

composition to enhance the performance and stability of the photovoltaic cells.<sup>[1–3]</sup> Mixed halide perovskites with Cl<sup>−</sup> and Br<sup>−</sup> were employed from the early times impacting on the optoelectronic properties of the material.<sup>[4,5]</sup> The role of chloride has been revealed in a longer carrier diffusion length, suppression of halide segregation, and increasing of the grain size and crystallinity.<sup>[6,7]</sup> Regarding the partial substitution of bromide for iodide, a better control of the growth of the perovskite is achieved together with a decreasing yield of superoxide species upon illumination which generates solar cells with record efficiency and greater stability.<sup>[8]</sup> As for the use of lead as the typical divalent cation in the structure of the hybrid halide perovskite, it causes some concerns due to the environmental toxicity of this metal.<sup>[9–11]</sup> Thus, replacement of the Pb<sup>2+</sup> cation by the harmless Sn<sup>2+</sup> has been extensively reported, although its facile oxidation to Sn<sup>4+</sup> produces a high density of defects with a related lower performance and

stability.<sup>[12]</sup> However, the wider variation in the composition of the archetypal MAPbI<sub>3</sub> perovskite has occurred in the MA cation (A-cation) which is determined by the Goldsmith tolerance factor.<sup>[13]</sup>

The A-site cation engineering approach has revealed as an elegant tool to enhance the performance and, more importantly, to extend the stability of 3D hybrid perovskite solar cells.<sup>[14,15]</sup> Cesium (Cs) and formamidinium (FA) are the only two cations that can fully replace MA according to the geometrical restrictions imposed by the tolerance factor.<sup>[16,17]</sup> However, the stable phase at room temperature is not a 3D structure and therefore the valuable “black phase” for photovoltaics was needed to be stabilized in ambient conditions.<sup>[18]</sup> Moreover, combination of these three size allowed cations (MA, FA, and Cs) has resulted in an optimized performance of the solar cells due to suppression of the undesired yellow phases and favoring a seed-assisted crystal growth, e.g., Cs<sub>0.1</sub>(FA<sub>0.83</sub>MA<sub>0.17</sub>)<sub>0.9</sub>Pb(I<sub>0.83</sub>Br<sub>0.17</sub>)<sub>3</sub>.<sup>[19]</sup>


The next rational strategy has been the partial incorporation of out-of-tolerance factor cations into the 3D structure of hybrid perovskites<sup>[20]</sup> which has been recently extended to 2D Ruddlesden–Popper perovskites.<sup>[21,22]</sup> Several cations including rubidium (Rb), potassium (K), ethylammonium (EA), and guanidinium (Gua) have been successfully incorporated into the octahedral voids forming mixed A-cation 3D perovskites with variable

## 1. Introduction

As the initial articles reported the successful utilization of the methylammonium lead iodide (MAPbI<sub>3</sub>) perovskite in solar devices, several attempts have been performed to modify its

S. Ramos-Terrón, J. F. Illanes, D. Bohoyo-Gil, L. Camacho, G. de Miguel  
Departamento de Química Física y Termodinámica Aplicada, Instituto  
Universitario de Investigación en Química Fina y Nanoquímica, IUNAN  
Universidad de Córdoba  
Campus de Rabanales, Edificio Marie Curie, E-14071 Córdoba, Spain  
E-mail: gmiguel@uco.es

D. Bohoyo-Gil  
Departamento de Química Orgánica, Instituto Universitario de  
Investigación en Química Fina y Nanoquímica, IUNAN  
Universidad de Córdoba  
Campus de Rabanales, Edificio Marie Curie, E-14071 Córdoba, Spain

 The ORCID identification number(s) for the author(s) of this article can be found under <https://doi.org/10.1002/solr.202100586>.

© 2021 The Authors. Solar RRL published by Wiley-VCH GmbH. This is an open access article under the terms of the Creative Commons Attribution-NonCommercial License, which permits use, distribution and reproduction in any medium, provided the original work is properly cited and is not used for commercial purposes.

DOI: 10.1002/solr.202100586

contents (<30%) of the A-cation.<sup>[23–25]</sup> It is particularly positive the effect of the inclusion of Gua into the  $\text{MA}_{1-x}\text{Gua}_x\text{PbI}_3$  ( $x < 0.2$ ) structure on the efficiency and, specially, the stability of the solar cells due to formation of additional hydrogen bonds by the Gua cation.<sup>[14,26,27]</sup> The enhanced resistance to degradation due to Gua inclusion has stimulated its use in the record-breaking triple cation  $\text{Cs}_{0.1}(\text{FA}_{0.83}\text{MA}_{0.17})_{0.9}\text{Pb}(\text{I}_{0.83}\text{Br}_{0.17})_3$  perovskite.<sup>[28]</sup> Thus, few reports have recently established the formation of a quadruple cation perovskite with the Gua cation passivating bandgap defects which enhances the open-circuit voltage ( $V_{oc}$ ).<sup>[29]</sup> However, no detailed analysis has been performed on the incorporation of Gua into double cation perovskites which may elucidate the interplay among the different A-cations.

In this study, we investigate the structural and optoelectronic impact of the incorporation of the Gua cation into the double cation  $\text{Cs}_x\text{MA}_{1-x}\text{PbI}_3$  perovskite to generate a triple cation  $\text{Cs}_x\text{Gua}_y\text{MA}_{1-x-y}\text{PbI}_3$  perovskite. The X-ray diffraction (XRD) measurements have demonstrated the opposite effect of the small Cs and large Gua cations on the dimension of the perovskite unit cell. Thus, the shrinkage of the perovskite unit cell produced by the incorporation of the Cs cations is reverted upon addition of the Gua cations which expand the size of the lattice constants. Time-resolved photoluminescence (PL) measurements display different time constants depending on the composition of the A-cation which are line to the trap density calculated in the space charge limited current (SCLC) experiments. The measured performance and stability of the solar devices fabricated with the different mixed cation  $\text{Cs}_x\text{Gua}_y\text{MA}_{1-x-y}\text{PbI}_3$  perovskites reveal a beneficial impact on both parameters due to the incorporation of the Gua cations in opposition to the negative effect of the Cs cations.

## 2. Results

The incorporation of the Cs cations into the  $\text{MAPbI}_3$  perovskite has been studied to characterize the structural changes in the crystal lattice. **Figure 1A** displays the overall XRD measurement of the  $\text{MAPbI}_3$  perovskite (black line) containing all reflection peaks assigned to the tetragonal phase ( $I4/mcm$ ).<sup>[30]</sup> The peaks at  $26.51^\circ$  and  $37.77^\circ$  correspond to the fluorine tin oxide (FTO) substrate employed as the reference position.

The addition of a low content of Cs replacing the MA cation (5% and 15%) does not apparently modify the XRD pattern which indicates that the tetragonal structure of the  $\text{MAPbI}_3$  perovskite is conserved in line with a previously published work reporting the inclusion of until 5% of Cs in single crystals of the  $\text{MAPbI}_3$  perovskite.<sup>[17]</sup> **Figure 1B** shows a magnification of the more intense Bragg peaks associated to the (110) and (220) planes, clearly exhibiting a shift of the peaks to larger angles at increasing content of Cs. This result indicates a shrinkage of the unit cell due to the partial substitution of the MA by the smaller Cs cations which demonstrates that Cs cations are incorporated up to a 15% in  $\text{MAPbI}_3$  thin films. This value is larger than the typical 5% employed in the record-breaking triple cation  $\text{CsMAFA}$  perovskites for photovoltaics.<sup>[19,31]</sup> In addition to the observed shift of the reflection peaks, a decrease of the signal together with a broadening of the peaks is detected. The lower XRD signal is associated to a decrease in the crystallinity of the films and the broader full width at half maximum (FWHM) can be ascribed to a distortion of the crystal or to a smaller size of the nanocrystals. As the scanning electron microscopy (SEM) images display similar crystallite sizes (see below), the larger bandwidth of the reflection peaks at higher content of the Cs cation is accounted for an increased number of microstrain and distortions of the  $\text{MAPbI}_3$  lattice due to the Cs incorporation. The increase of the lattice strain is generally responsible for the formation of atomic vacancies which, in turn, may affect to the performance and stability of these mixed A-cation perovskites.<sup>[20]</sup>

The addition of the Gua cation into the precursor solution together with the MA cation has previously been reported to yield the 3D mixed A-cation  $\text{MA}_{1-x}\text{Gua}_x\text{PbI}_3$  perovskite up to a percentage of 25% Gua.<sup>[14]</sup> At higher Gua content, low-dimensional phases are formed due to the strong distortion of the 3D crystal lattice. **Figure S1**, Supporting Information, exhibits the shift to lower  $2\theta$  angles of the (110) and (220) XRD peaks at increasing content of the Gua cation (0–15%) which demonstrates the expansion of the unit cell due to the larger size of Gua with respect to the MA cation.

Once the independent incorporation of the Cs or Gua cations into the octahedral voids of the  $\text{MAPbI}_3$  perovskite is characterized, both Cs and Gua cations are included together in the precursor solution with MA to accomplish the formation of a triple A-cation  $\text{Cs}_x\text{Gua}_y\text{MA}_{1-x-y}\text{PbI}_3$  perovskite. **Figure 2** displays the

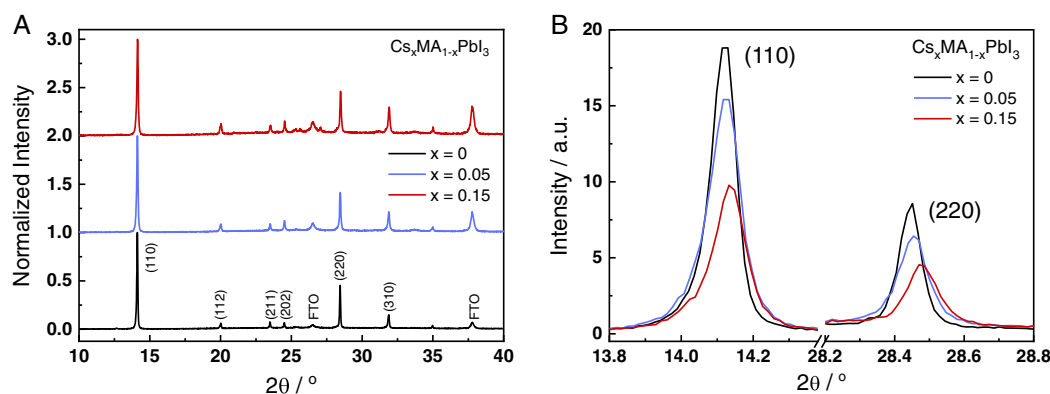


**Figure 1.** A) Full range and B) close view of the main reflection peaks of the XRD measurements of mixed A-cation  $\text{Cs}_x\text{MA}_{1-x}\text{PbI}_3$  perovskite films.

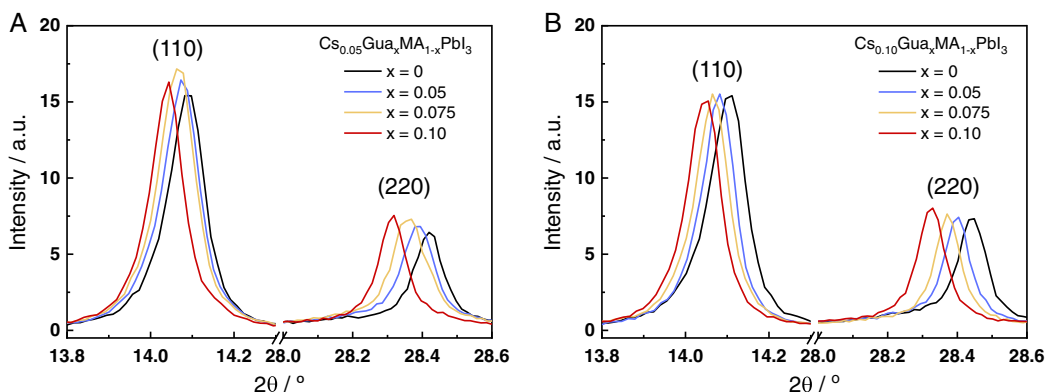


**Figure 2.** Bragg peaks corresponding to the (110) and (220) planes at different contents of the Gua cation in a  $\text{Cs}_x\text{Gua}_y\text{MA}_{1-x-y}\text{PbI}_3$  perovskite film with A)  $x = 0.05$  and B)  $x = 0.10$ .

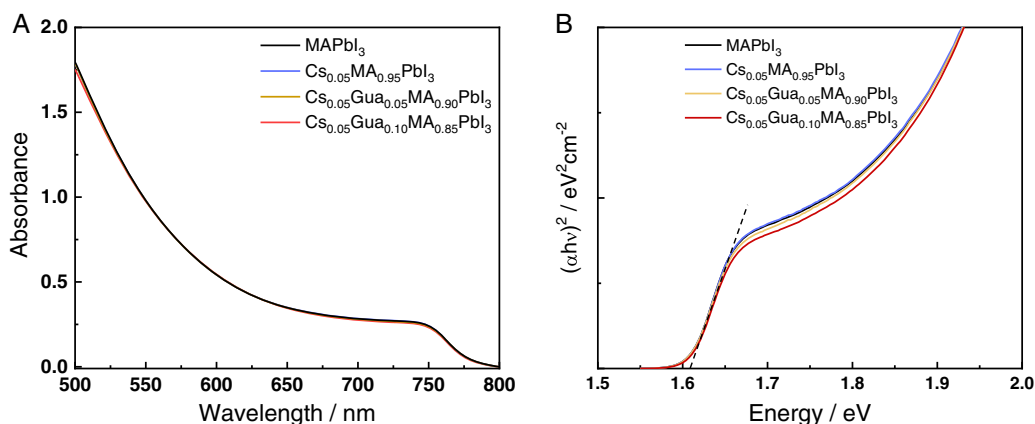
effect of the sequential addition of Gua (0–10%) on the XRD main Bragg peaks at two different concentrations of the Cs cation, 5% and 10%, in Figure 2A,B, respectively. A gradual shift to lower  $2\theta$  angles is clearly observed when increasing the Gua content up to a 10% value. Moreover, the intensity and width of both XRD peaks are maintained which indicates similar crystallinity and local strain at the different Gua content. This result reveals that the addition of Gua in the mixed A-cation  $\text{Cs}_x\text{MA}_{1-x}\text{PbI}_3$  produces the same expansion of the unit cell as it was previously described in the  $\text{MAPbI}_3$  perovskite. Thus, at the low content of Cs and Gua shown in Figure 2, the 3D inorganic  $\text{PbI}_6$  network is able to accommodate the three cations with variable sizes. It is worth mentioning that the presence of the large Gua cations together with the small Cs cations does not introduce an additional strain in the lattice as it was described in the discrete incorporation of Cs or Gua. Thus, the strain produced by the addition of the Gua cation is compensated in the triplet A-cation perovskite by the presence of the smaller Cs cation.

Figure S2, Supporting Information, displays the two reflection peaks of the (110) and (220) crystallographic planes for the mixed A-cation  $\text{Cs}_x\text{Gua}_y\text{MA}_{1-x-y}\text{PbI}_3$  perovskite films with (5%) and without the Cs cation at different contents of the Gua cation. These graphs allow one to clearly identify the shift to larger angles associated to the addition of 5% of the Cs cation in all

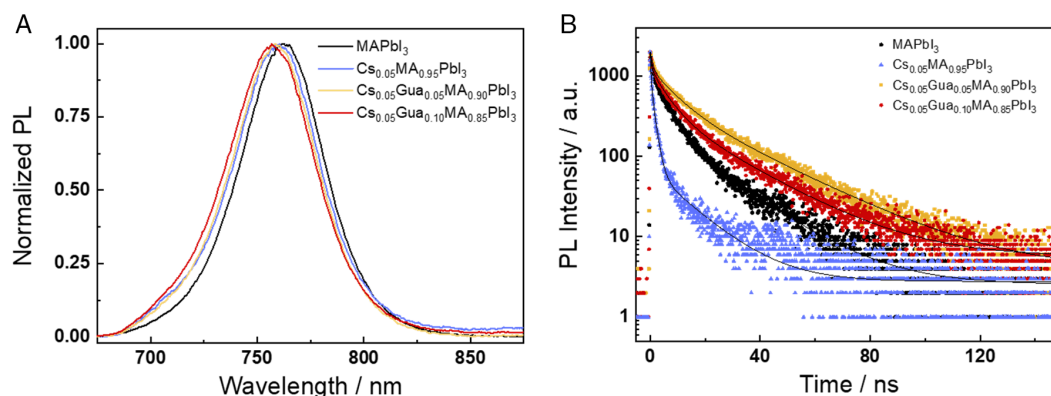
samples. The inclusion of the Cs cation into the mixed A-cation  $\text{MA}_{1-x}\text{Gua}_x\text{PbI}_3$  perovskite is demonstrated as it was previously described for the  $\text{MAPbI}_3$  films. Thus, both Cs and Gua cations can jointly be inserted into the octahedral voids of the 3D perovskites at the percentages studied here, causing a reduction or expansion of the unit cell, respectively.

Figure 3A displays the absorbance spectra for the mixed A-cation  $\text{Cs}_x\text{Gua}_y\text{MA}_{1-x-y}\text{PbI}_3$  perovskite films with different percentage of the Cs or Gua cations. The spectra exhibit similar absorption onset at 750 nm with increasing absorption towards the lower wavelength region. Tauc plots are presented in Figure 3B assuming a direct bandgap for the optical transition. The extrapolation of the straight line according to the Tauc procedure to the zero value displays very similar bandgap energies ( $E_g = 1.61$  eV) for all mixed A-cation perovskites. Apparently, the incorporation of Gua seems to modify the  $E_g$  providing a slight larger value as previously reported.<sup>14</sup> In any case, the absorption ability of all mixed A-cations perovskites with moderate percentages of Cs (5%) or Gua (10%) is maintained which is highly beneficial for the fabrication of photovoltaic devices.

The measurement of the PL of the different mixed A-cation perovskites provides valuable information of the charge carrier dynamics. Figure 4A displays the typical steady-state PL band ( $\lambda_{\text{exc}} = 400$  nm) centered at 762 nm for the  $\text{MAPbI}_3$  perovskites.



**Figure 3.** A) Absorbance and B) Tauc plots of the mixed A-cation  $\text{Cs}_x\text{Gua}_y\text{MA}_{1-x-y}\text{PbI}_3$  perovskite films.



**Figure 4.** A) Steady-state and B) time-resolved PL of the mixed A-cation  $\text{Cs}_x\text{Gua}_y\text{MA}_{1-x-y}\text{PbI}_3$  perovskite films.  $\lambda_{\text{exc}} = 400$  nm.

We observe slight blueshift of the maximum of the PL peak when adding the Cs and the Cs/Gua cations ( $\lambda_{\text{PL}} = 757\text{--}760$  nm). This behavior previously reported in the  $\text{Gua}_x\text{MA}_{1-x}\text{PbI}_3$  perovskite was attributed to a more negative value in the valence band energies.<sup>[14]</sup> Our results indicate that Cs cation also modifies the energy of the bandgap in the  $\text{MAPbI}_3$  perovskite and this effect is still active upon addition of Gua cation in the mixed A-cation  $\text{Cs}_x\text{Gua}_y\text{MA}_{1-x-y}\text{PbI}_3$  perovskite films. The slight increase of the bandgap energy in the triple A-cation perovskites might induce a larger open-circuit voltage ( $V_{\text{oc}}$ ) value in the solar devices prepared with this type of materials with respect to those fabricated with the  $\text{MAPbI}_3$  perovskite. Figure 4B displays the PL decays of the different mixed A-cation perovskites exciting at 400 nm ( $E_{\text{pulse}} = 100 \mu\text{J cm}^{-2}$ ). The  $\text{MAPbI}_3$  films exhibit PL decays that are fitted with a triexponential function delivering an average time constant of  $\tau_{\text{av}} = 11.6$  ns, while the  $\text{Cs}_{0.05}\text{MA}_{0.95}\text{PbI}_3$  perovskite films display shorter decays with  $\tau_{\text{av}} = 9.0$  ns. The shorter decay in the Cs-containing mixed A-cation perovskite reveals a larger charge carrier recombination. On the contrary, the PL decays in the Gua-containing perovskites are longer compared to those of the  $\text{MAPbI}_3$  perovskite, indicating a slower charge carrier recombination. In particular, the average time constants of  $\tau_{\text{av}} = 19.6$  ns and  $\tau_{\text{av}} = 17.0$  ns are obtained for the films containing 5% and 10% of Gua, respectively. The different PL time constants which are linked to the dynamics of the charge recombination process are expected to impact the efficiency of the perovskite solar cells (PSCs).

To get an insight into the origin of the different PL time constants, we have performed SEM measurements to investigate the morphology of the crystalline perovskite layers and we have studied the defect states with the SCLC method. Figure S3, Supporting Information, shows the SEM images of the thin layers of mixed cation perovskites. In all cases, full coverage of the surface is observed with absence of pinholes that would be detrimental for the performance of the fabricated PSCs. The deposited layers are arranged in a densely packed grain structure with a size of the grains in the range of 200–400 nm. The grain boundaries are very smooth with no differences among all four samples. Thus, the partial incorporation of Cs or Gua to the 3D  $\text{MAPbI}_3$  perovskite does not apparently modify the morphology of the films at least at the low percentages utilized in this work. The similar number of grain boundaries in the

four mixed cation perovskites ensures that the carrier recombination sites are comparable in all samples<sup>[32]</sup> and therefore the different PL time decays are not explained due to changes in the morphology/boundaries of the perovskite grains.

The SCLC method was also utilized to study the concentration of defect state in the bulk of the material. Figure 5 displays the dark  $J$ – $V$  curves for electron-only devices with a structure of FTO/ $\text{c-TiO}_2$ /perovskite/PCBM/Au. The increase of the applied voltage clearly defines three regions with different slopes in the  $J$ – $V$  curves (log scale): an Ohmic region with slope  $n = 1$ , a trap-filling limited (TFL) region with  $n > 3$ , and a child region with  $n = 2$ . The trap densities close to the conduction band minimum (CBM) can be calculated from the voltage ( $V_{\text{TFL}}$ ), marking the transition between the Ohmic region and the TFL region by using Equation (1)

$$V_{\text{TFL}} = \frac{en_1L^2}{2\epsilon\epsilon_0} \quad (1)$$

where  $e$  is the electron charge,  $n_1$  is the trap density,  $L$  is the thickness of the perovskite layer (400 nm),  $\epsilon$  is the relative dielectric constant (70 for the perovskites),<sup>[33]</sup> and  $\epsilon_0$  is the dielectric constant of the vacuum.<sup>[34]</sup> Table S1, Supporting Information, collects the slopes of all linear fits for the three regions. We have obtained a value of trap density of  $1.7 \times 10^{16} \text{ cm}^{-3}$  for the films of  $\text{MAPbI}_3$  perovskite which is in good agreement with the reported values for a high crystalline layer of this material.<sup>[35]</sup> It is worth mentioning that the obtained trap density is larger compared to that value reported in single crystals.<sup>[36]</sup> Indeed, the surface trap states are expected to dominate in films compared to high-quality crystals.<sup>[37]</sup> In the mixed cation  $\text{Cs}_{0.05}\text{MA}_{0.95}\text{PbI}_3$  perovskite layer, the trap density increases to  $2.4 \times 10^{16} \text{ cm}^{-3}$  while in the  $\text{Cs}_{0.05}\text{Gua}_{0.05}\text{MA}_{0.90}\text{PbI}_3$  perovskite the trap density decreases to a value of  $1.2 \times 10^{16} \text{ cm}^{-3}$ , both values compared with that of the reference sample. Finally, we found a similar value of  $1.7 \times 10^{16} \text{ cm}^{-3}$  for the trap density of the mixed cation  $\text{Cs}_{0.05}\text{Gua}_{0.10}\text{MA}_{0.85}\text{PbI}_3$  perovskite as in the  $\text{MAPbI}_3$ . The SCLC measurements reveal that the incorporation of Cs to the 3D perovskite adds defects to the structure while the addition of the Gua cation produces the opposite effect, a decrease of the density of defects. The higher lattice strain observed in the XRD measurements for the films with only Cs already indicated a potential higher concentration of trap defects. These results

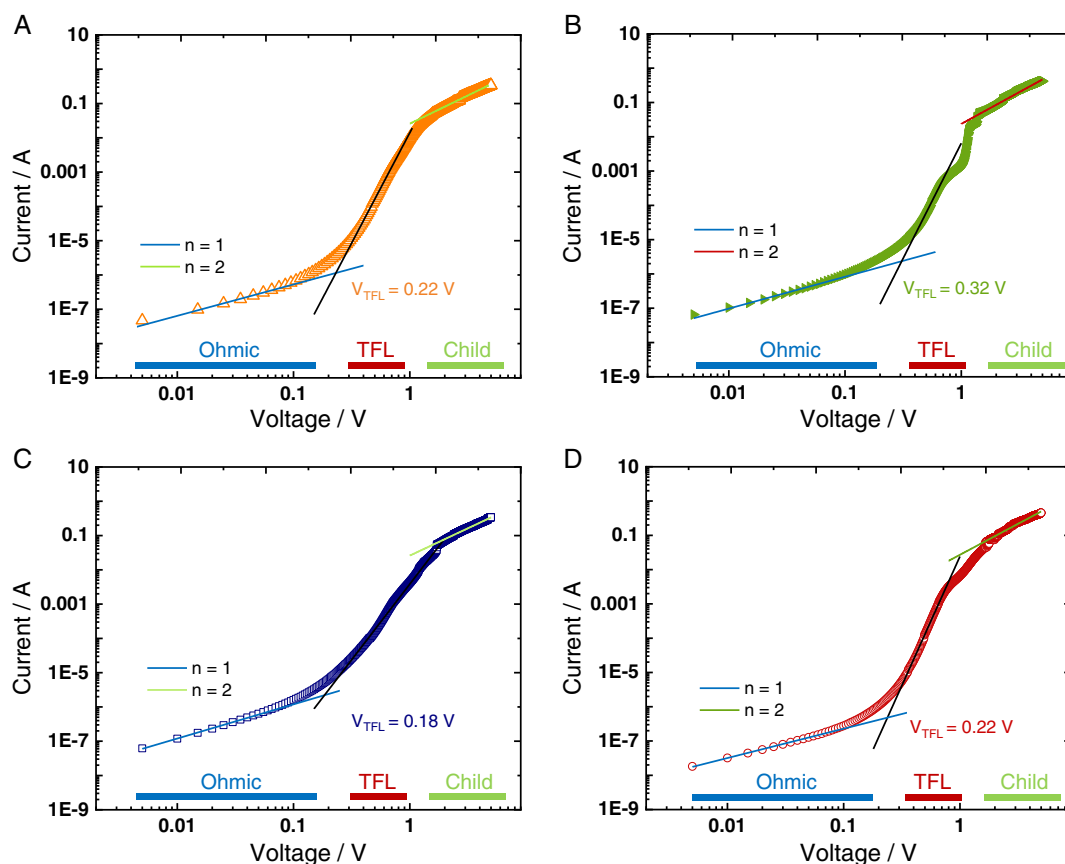


**Figure 5.** Dark  $J$ - $V$  curves for electron-only devices of the mixed cation perovskites: A) MAPbI<sub>3</sub>, B) Cs<sub>0.05</sub>MA<sub>0.95</sub>PbI<sub>3</sub>, C) Cs<sub>0.05</sub>Gua<sub>0.05</sub>MA<sub>0.90</sub>PbI<sub>3</sub>, and D) Cs<sub>0.05</sub>Gua<sub>0.10</sub>MA<sub>0.85</sub>PbI<sub>3</sub>.

account for the changes in the PL time constants observed in the time-resolved measurements. The shorter PL time decay in the mixed cation perovskite with only Cs is explained due to a higher trap density while the longer PL time decay of the sample with 5% of Gua is ascribed to a lower density of traps in that film. Thus, the obtained results should be very valuable to interpret the changes in the performance of the solar cells prepared with each type of mixed cation perovskites.

The electron mobility ( $\mu$ ) can be also calculated for each perovskite film from the dark  $J$ - $V$  curves by fitting the experimental values at the child region to the Mott-Gurney law (Equation (2))

$$\mu = \frac{8JL^3}{9\epsilon\epsilon_0 V^2} \quad (2)$$

where  $J$  is the current density and  $V$  is the applied voltage. The obtained electron mobilities are very similar to each other with values of 3.8, 4.5, 3.8, and 4.9 cm<sup>2</sup> V<sup>-1</sup> s<sup>-1</sup> for MAPbI<sub>3</sub>, Cs<sub>0.05</sub>MA<sub>0.95</sub>PbI<sub>3</sub>, Cs<sub>0.05</sub>Gua<sub>0.05</sub>MA<sub>0.90</sub>PbI<sub>3</sub>, and Cs<sub>0.05</sub>Gua<sub>0.10</sub>MA<sub>0.85</sub>PbI<sub>3</sub>, respectively. Apparently, the addition of Cs or Gua does not introduce any tendency in the electron mobility values.

PSCs were fabricated to evaluate the influence of the partial incorporation of the Cs and Gua cation on the performance of the cells. The  $n$ - $i$ - $p$  mesoscopic configuration was preferred as the architecture of the cells with TiO<sub>2</sub> blocking and a TiO<sub>2</sub>

mesoporous films as electron transport layers (ETL) and Spiro-MeOTAD as the hole transport layer (HTL). **Figure 6** illustrates the  $J$ - $V$  curves for each champion device upon illumination with a solar simulator. **Figure 7** displays the average photovoltaic parameters obtained from the cells, which also includes the champion cells obtained for each condition. An average power conversion efficiency (PCE) of 18.6% was obtained for the cells fabricated with the reference MAPbI<sub>3</sub> perovskite, comparable with those obtained for the best representative MAPbI<sub>3</sub>-based PSCs reported in the literature.<sup>[38]</sup> The PCE value of the cells containing the Cs<sub>0.05</sub>MA<sub>0.95</sub>PbI<sub>3</sub> perovskite layer is considerably lower, 17.3%, due to a decreased  $V_{OC}$  but specially a reduced value of the fill factor (FF). On the contrary, the addition of 5% or 10% Gua into the triple cation perovskite produces an increase of the PCE to a value of 20.0% and 19.0%, respectively. All photovoltaic parameters are larger compared to the reference MAPbI<sub>3</sub> perovskite, especially the  $V_{OC}$ . This phenomenon is explained due to the slight increase in the bandgap energy ( $E_g$ ) upon increasing the content of Gua which has been previously reported.<sup>[14]</sup> The minor distortions of the crystal lattice produced by the incorporation of the Gua cations affect the position of the valence and conduction band and therefore the bandgap energy. This phenomenon is similar to that observed in the hybrid halide perovskites containing Br as the halide anion (MAPbBr<sub>3</sub>) where the larger  $E_g$  value compared to the iodide perovskites is related to a larger  $V_{OC}$ .<sup>[39]</sup> Thus, the

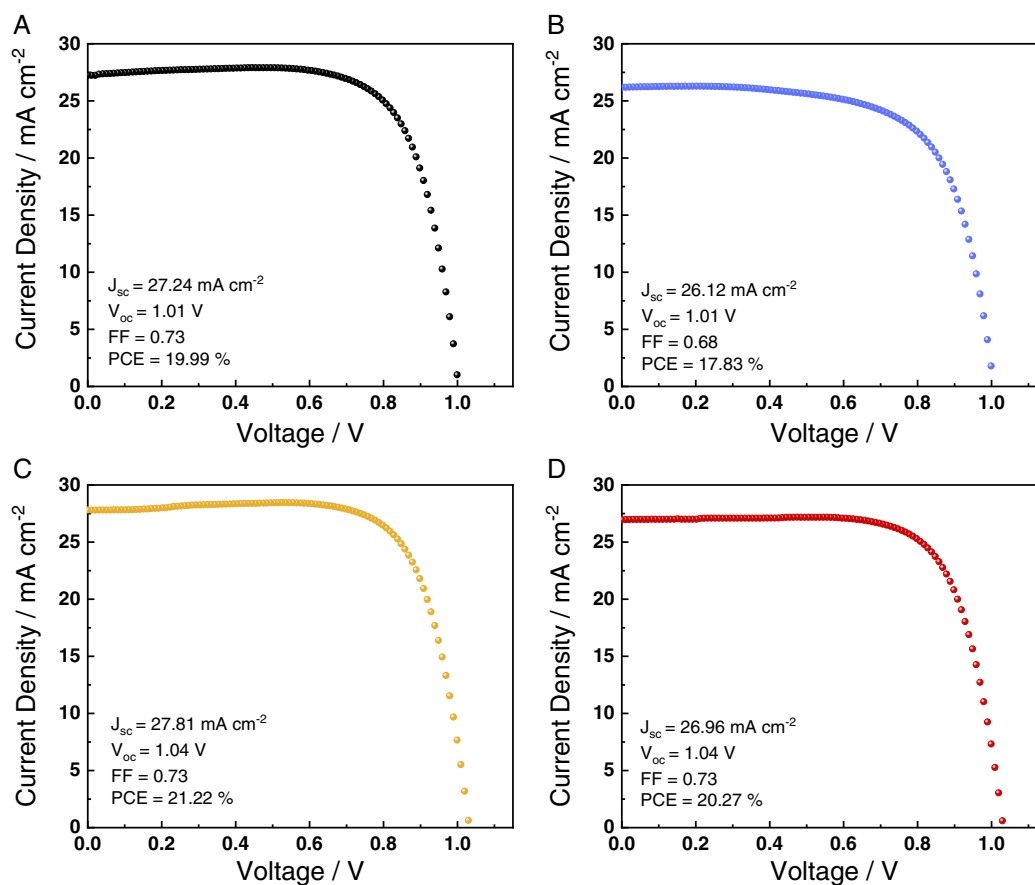


**Figure 6.**  $J$ - $V$  curves of the champion solar devices prepared with different mixed cation perovskites: A) MAPbI<sub>3</sub>, B) Cs<sub>0.05</sub>MA<sub>0.95</sub>PbI<sub>3</sub>, C) Cs<sub>0.05</sub>Gua<sub>0.05</sub>MA<sub>0.90</sub>PbI<sub>3</sub>, and D) Cs<sub>0.05</sub>Gua<sub>0.10</sub>MA<sub>0.85</sub>PbI<sub>3</sub>.

inclusion of Gua into the 3D structure of the perovskite is capable of reverting the negative effect of the Cs cations on the performance of the perovskite solar cells. The tendency in the PCE values matches well with the PL time decays for each type of perovskite. We have obtained larger PCE values for those mixed cation perovskites with longer PL time constants as a consequence of the lower density of trap states.

In addition to the changes in the performance of the solar cells when adding Cs or Gua to the 3D MAPbI<sub>3</sub> perovskite, the stability of the material and, therefore, of the devices is also affected. The stability of the solar cells is tested in devices without encapsulation which reveals a more intense degradation compared to reported encapsulated devices. Figure S4, Supporting Information, reflects the reduction of the initial PCE value of PSCs stored at room temperature and ambient atmosphere. After the initial 50 h, a significance decrease of the PCE is observed in all samples, which is normally attributed to the interpenetration of spiro-OMeTAD and gold electrode.<sup>[40]</sup> Then, the PCE of the samples containing Gua is gradually stabilized while it follows decreasing for the reference or Cs-only containing devices. After 600 h, the PCE is 50–55% of the initial one in the mixed cation perovskites with Gua while it is only 30% in the reference MAPbI<sub>3</sub> perovskite. Our results reveal that Cs does not assist in the stabilization of the 3D perovskite but Gua does, with a higher

PCE value at larger content of Gua. The presence of three amino groups in the Gua allows the formation of additional H-bonds with the octahedral iodide stabilizing the 3D structure.<sup>[14]</sup>

### 3. Conclusions

The addition of small percentages of Cs or Gua (5–10%) into the precursor solution to fabricate the 3D perovskites resulted in a shift of the Bragg reflection peaks with respect to those found in the MAPbI<sub>3</sub> perovskite to higher or lower  $2\theta$  angles, respectively. These results demonstrate a shrinkage of the unit cell due to the incorporation of Cs that can be reverted if Gua cations are added together with the Cs cations, forming a triple cation Cs<sub>x</sub>Gua<sub>y</sub>MA<sub>1-x-y</sub>PbI<sub>3</sub> perovskite. The subtle changes in the structure of the 3D perovskite entail a modification of the PL time decays that are explained due to different trap density. Thus, the addition of Cs cations into the structure appears to increase the density of trap states shortening the charge carrier lifetime. On the other hand, the inclusion of Gua into the 3D perovskite decreases the trap density retarding the charge carrier recombination. Our results reveal the structure–property relationship in the Cs/Gua mixed cation 3D perovskites. Finally, the PSCs fabricated with these materials display PCE in line with the

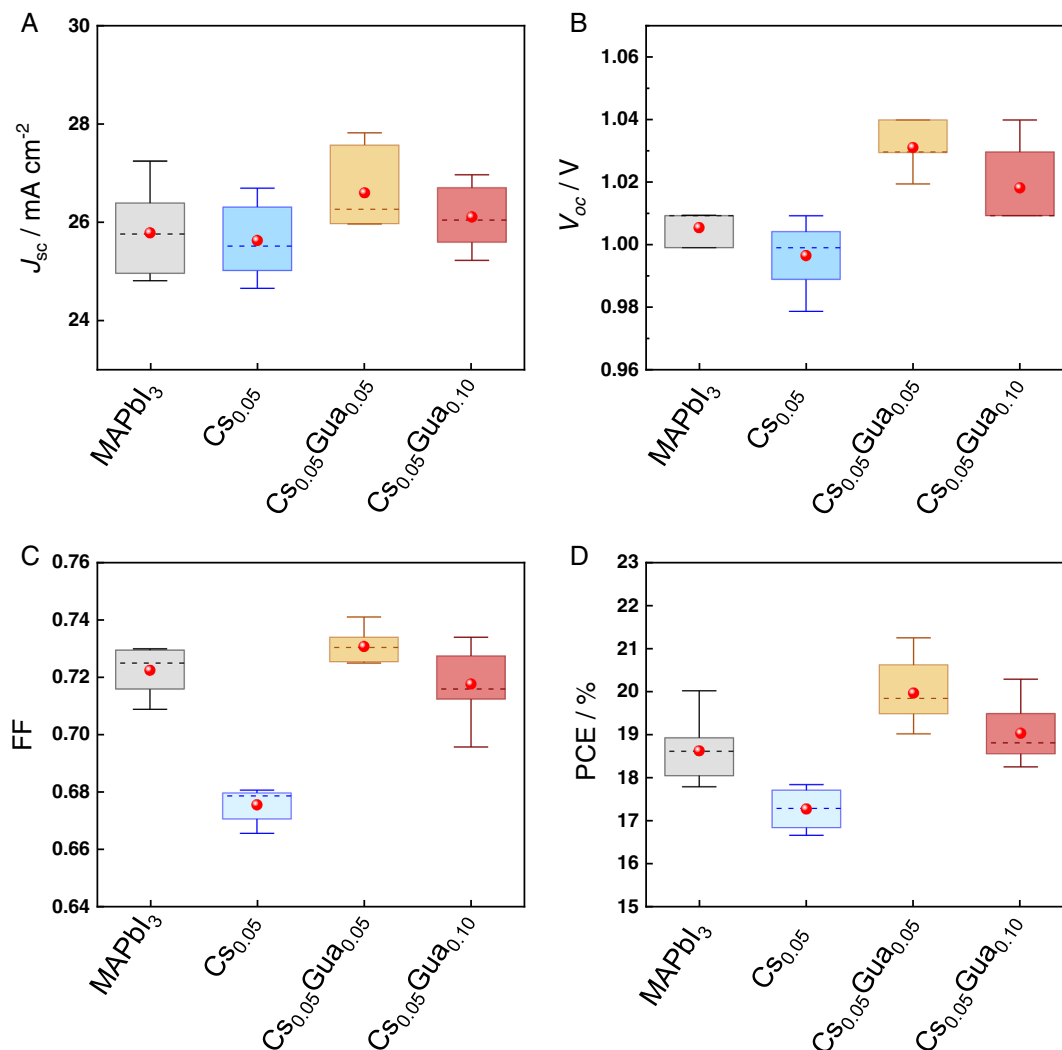


**Figure 7.** Statistical data for A)  $J_{sc}$ , B)  $V_{oc}$ , C) FF, and D) PCE obtained from more than 20 cells prepared with the mixed cation  $Cs_xGua_yMA_{1-x-y}PbI_3$ . The top bar shows the maximum value, the bottom bar shows the minimum value, the circle shows the mean value, and the dashed rectangle shows the region containing 25–75% of the data, obtained for each condition.

optoelectronic properties. The PCE rises from an average value of 18.6% in the MAPbI<sub>3</sub>-based device to a value of 20.0% in the Cs<sub>0.05</sub>Gua<sub>0.05</sub>MA<sub>0.90</sub>PbI<sub>3</sub>-based perovskite while it decreases to 17.3% in the device containing the double cation Cs<sub>0.05</sub>MA<sub>0.95</sub>PbI<sub>3</sub> perovskite.

#### 4. Experimental Section

**Starting Materials:** Lead iodide (PbI<sub>2</sub>, 99%), methylammonium iodide (MAI, 98%), guanidinium iodide (GuaI, 99%), cesium iodide (CsI, 99.999%), titanium diisopropoxide bis(acetylacetonate) solution (75% in 2-propanol), spiro-MeOTAD, 4-*tert*-butylpyridine (TBP), lithium bis(trifluoromethylsulfonyl)imide (LiTFSI), cobalt (III) FK209 TFSI, [6,6]-phenyl C<sub>61</sub> butyric acid methyl ester (PCBM), and acetonitrile (ACN, 99.9%) were supplied by Sigma-Aldrich. *N,N*-dimethylformamide (DMF, 99.8%) extra dry over molecular sieve, AcroSeal, dimethyl sulfoxide (DMSO, 99.7%) extra dry over molecular sieve, AcroSeal, and chlorobenzene extra dry over molecular sieve, AcroSeal were purchased from Acros Organics. Ethanol

absolute dry (maximum 0.02% water) and TiO<sub>2</sub> paste (DSL 30 NR-D, batch 438) were purchased from PanReac AppliChem and Dyesol, respectively. The glass patterned with FTO TEC-15 was purchased from Pilkington. Isopropyl alcohol (technical grade, 99.5%) and soap (decon90) were purchased from PanReac AppliChem and Decon, respectively.

**Devices Fabrication:** All substrates were cleaned by a sequential sonication treatment in Decon 90, Milli-Q water, and isopropyl alcohol, followed by UV-ozone treatment for 15 min.

**Solar Devices:** The structure device given FTO/c-TiO<sub>2</sub>/m-TiO<sub>2</sub>/perovskite/Spiro/Au was fabricated. A compact blocking layer of TiO<sub>2</sub> (c-TiO<sub>2</sub>, 30 nm in thickness) was deposited onto the FTO glass substrate by spray pyrolysis, using a titanium diisopropoxide bis(acetylacetonate) solution in ethanol (60% v/v). c-TiO<sub>2</sub> layer was then kept at 450 °C for 30 min for formation of anatase phase.<sup>[41]</sup> The mesoporous TiO<sub>2</sub> layer (m-TiO<sub>2</sub>, 200 nm in thickness) was deposited by spin coating at 2000 rpm for 15 s using a diluted TiO<sub>2</sub> dispersion in ethanol, ratio 1:8 by weight. m-TiO<sub>2</sub> layer was sintered at 500 °C for 30 min and later cooled to room temperature.<sup>[42]</sup> Stoichiometric precursor solution was prepared by mixing MAI, GuaI, CsI, and PbI<sub>2</sub> in DMF/DMSO. The concentration of the precursors in the solution was adjusted to the relative humidity of the

environment (40% RH) by the Pb/DMSO ratio, keep the  $\text{PbI}_2$  molarity equal to 1.35.<sup>[42]</sup>

The perovskite films have been deposited using a spin coating process previously reported.<sup>[43]</sup> The perovskite precursor solution (50  $\mu\text{L}$ ) was deposited on the  $\text{m-TiO}_2$  layer at 4000 rpm for 50 s. During this step, 200  $\mu\text{L}$  of chlorobenzene was poured onto the films and the films were annealed at 100 °C on a hot plate for 20 min. After this, spiro-OMeTAD was spin-coated at 400 rpm for 30 s from a chlorobenzene solution (28.9 mg in 400  $\mu\text{L}$ ) containing LiTFSI (7.0  $\mu\text{L}$  from a 520  $\text{mg mL}^{-1}$  stock solution in acetonitrile), TBP (11.5  $\mu\text{L}$ ), and Co(III)TFSI (8.8  $\mu\text{L}$  from a 40  $\text{mg mL}^{-1}$  stock solution) as dopants. Finally, a 70 nm gold electrode was deposited as a metallic contact by thermal evaporation ( $1 \times 10^{-6}$  Torr).

**Electron-Only Devices:** The structure device given FTO/ $\text{c-TiO}_2$ /perovskite/PCBM/Au was fabricated. All layers have been deposited following the steps detailed above. PCBM chlorobenzene solution (10  $\text{mg mL}^{-1}$ ) was spin-coated on perovskite films. After this, the films were annealed at 100 °C for 10 min.<sup>[44]</sup>

**XRD Measurements:** XRD experiments were performed using a Bruker D8 DISCOVER diffractometer operating at 40 kV and 40 mA and using  $\text{Cu K}\alpha$  radiation (1.54060 Å). The range of measurement was done from 2° to 40° Bragg angles.

**UV-vis Absorption Spectroscopy:** UV-vis absorption spectra were performed at room temperature ( $\approx 25$  °C) using a Cary 100 UV-vis spectrophotometer in the range of 500–800 nm in all cases.

**Steady-State and Time-Resolved PL Measurements:** Steady-state PL spectra were recorded with a FLS980 (Edinburgh Instruments) PL spectrometer using a 450 W Xenon arc lamp and a R298P photomultiplier as detector. Time-resolved fluorescence measurements were accomplished through the time-correlated single photon counting (TCSPC) technique, by using the same FLS980 (Edinburgh Instruments) PL spectrometer. The samples were excited at 406.4 nm with an 86.8 ps pulse width diode laser using a R2658P photomultiplier as the detector.

**SEM Studies:** SEM image of the films was performed using a JEOL JSM 7800F microscope working at 2 kV. The work distances were  $\approx 10$  mm for all cases and 20 000 $\times$  magnification.

**Device Characterization:** The photovoltaic device performance was analyzed using an Oriel LSH-7320 ABA LED solar simulator producing 1 Sun  $\text{AM1.5}$  (1000  $\text{W m}^{-2}$ ) sunlight. Current–voltage curves were measured with a Keithley 2400 potentiostat at a reverse scan rate of 100  $\text{mV s}^{-1}$  and a sweep delay of 20 s. The solar cells were masked with a metal aperture of 0.09  $\text{cm}^2$  to define the active area. The cells were measured in air, at room temperature, and without encapsulation.

## Supporting Information

Supporting Information is available from the Wiley Online Library or from the author.

## Acknowledgements

S.R.T. thanks the Ministry of Education, Culture, and Sport for a FPU fellowship (FPU18/04452). This work was financially supported by the Ministerio de Ciencia e Innovación of Spain, through CTQ2017-84221-R project, as well as by the Andalusian Government of Spain, through UCO-1265871-R and UCO-1263193 projects, all cofinanced with FEDER funds. The authors also acknowledge to the SCAI-UCO service for the assistance with SEM analysis.

## Conflict of Interest

The authors declare no conflict of interest.

## Data Availability Statement

Research data are not shared.

## Keywords

3D materials, guanidinium, hybrid perovskites, solar cells

Received: July 28, 2021

Revised: October 20, 2021

Published online: November 10, 2021

- [1] N. J. Jeon, J. H. Noh, W. S. Yang, Y. C. Kim, S. Ryu, J. Seo, S. Il Seok, *Nature* **2015**, 517, 476.
- [2] F. Xu, T. Zhang, G. Li, Y. Zhao, *J. Mater. Chem. A* **2017**, 5, 11450.
- [3] N. Pellet, P. Gao, G. Gregori, T. Y. Yang, M. K. Nazeeruddin, J. Maier, M. Grätzel, *Angew. Chem., Int. Ed.* **2014**, 53, 3151.
- [4] Q. Chen, H. Zhou, Y. Fang, A. Z. Stieg, T. Bin Song, H. H. Wang, X. Xu, Y. Liu, S. Lu, J. You, P. Sun, J. McKay, M. S. Goorsky, Y. Yang, *Nat. Commun.* **2015**, 6, 1.
- [5] M. J. P. Alcocer, T. Leijtens, L. M. Herz, A. Petrozza, H. J. Snaith, *Science* **2013**, 342, 341.
- [6] Y. Wu, X. Li, S. Fu, L. Wan, J. Fang, *J. Mater. Chem. A* **2019**, 7, 8078.
- [7] J. Cho, P. V. Kamat, *Chem. Mater.* **2020**, 32, 6206.
- [8] A. Aziz, N. Aristidou, X. Bu, R. J. E. Westbrock, S. A. Haque, M. S. Islam, *Chem. Mater.* **2020**, 32, 400.
- [9] A. D. Jodlowski, D. Rodríguez-Padrón, R. Luque, G. de Miguel, *Adv. Energy Mater.* **2018**, 8, 1.
- [10] W. Ke, M. G. Kanatzidis, *Nat. Commun.* **2019**, 10, 1.
- [11] P. Su, Y. Liu, J. Zhang, C. Chen, B. Yang, C. Zhang, X. Zhao, *J. Phys. Chem. Lett.* **2020**, 11, 2812.
- [12] X. Liu, Y. Wang, T. Wu, X. He, X. Meng, J. Barbaud, H. Chen, H. Segawa, X. Yang, L. Han, *Nat. Commun.* **2020**, 11, 1.
- [13] C. J. Bartel, C. Sutton, B. R. Goldsmith, R. Ouyang, C. B. Musgrave, L. M. Ghiringhelli, M. Scheffler, *Sci. Adv.* **2019**, 5, 1.
- [14] A. D. Jodlowski, C. Roldán-Carmona, G. Grancini, M. Salado, M. Ralaiarisoa, S. Ahmad, N. Koch, L. Camacho, G. De Miguel, M. K. Nazeeruddin, *Nat. Energy* **2017**, 2, 972.
- [15] C. Hu, Y. Bai, S. Xiao, T. Zhang, X. Meng, W. K. Ng, Y. Yang, K. S. Wong, H. Chen, S. Yang, *J. Mater. Chem. A* **2017**, 5, 21858.
- [16] G. E. Eperon, G. M. Paternò, R. J. Sutton, A. Zampetti, A. A. Haghighirad, F. Cacialli, H. J. Snaith, *J. Mater. Chem. A* **2015**, 3, 19688.
- [17] S. Du, L. Jing, X. Cheng, Y. Yuan, J. Ding, T. Zhou, X. Zhan, H. Cui, *J. Phys. Chem. Lett.* **2018**, 9, 5833.
- [18] W. Hui, L. Chao, H. Lu, F. Xia, Q. Wei, Z. Su, T. Niu, L. Tao, B. Du, D. Li, Y. Wang, H. Dong, S. Zuo, B. Li, W. Shi, X. Ran, P. Li, H. Zhang, Z. Wu, C. Ran, L. Song, G. Xing, X. Gao, J. Zhang, Y. Xia, Y. Chen, W. Huang, *Science* **2021**, 371, 1359.
- [19] M. Saliba, T. Matsui, J. Y. Seo, K. Domanski, J. P. Correa-Baena, M. K. Nazeeruddin, S. M. Zakeeruddin, W. Tress, A. Abate, A. Hagfeldt, M. Grätzel, *Energy Environ. Sci.* **2016**, 9, 1989.
- [20] M. I. Saidaminov, J. Kim, A. Jain, R. Quintero-Bermudez, H. Tan, G. Long, F. Tan, A. Johnston, Y. Zhao, O. Voznyy, E. H. Sargent, *Nat. Energy* **2018**, 3, 648.
- [21] S. Ramos-Terrón, C. Verdugo-Escamilla, L. Camacho, G. De Miguel, *Adv. Optical Mater.* **2021**, 9, 2100114.
- [22] S. Ramos-Terrón, A. D. Jodlowski, C. Verdugo-Escamilla, L. Camacho, G. De Miguel, *Chem. Mater.* **2020**, 32, 4024.
- [23] S. Gholipour, A. M. Ali, J. P. Correa-Baena, S. H. Turren-Cruz, F. Tajabadi, W. Tress, N. Taghavinia, M. Grätzel, A. Abate, F. De



- Angelis, C. A. Gaggioli, E. Mosconi, A. Hagfeldt, M. Saliba, *Adv. Mater.* **2017**, 29, 1.
- [24] J. K. Nam, S. U. Choi, W. Cha, Y. J. Choi, W. Kim, M. S. Jung, J. Kwon, D. Kim, J. H. Park, *Nano Lett.* **2017**, 17, 2028.
- [25] P. Yadav, M. I. Dar, N. Arora, E. A. Alharbi, F. Giordano, S. M. Zakeeruddin, M. Grätzel, *Adv. Mater.* **2017**, 29, 1.
- [26] M. H. Alotaibi, Y. A. Alzahrani, N. Arora, A. Alyamani, A. Albadri, H. Albrithen, I. H. Al-Lehyani, S. M. Alenzi, A. Z. Alanzi, F. S. Alghamdi, S. M. Zakeeruddin, S. Meloni, M. I. Dar, M. Graetzel, *Sol. RRL* **2020**, 4, 1.
- [27] L. Gao, X. Li, Y. Liu, J. Fang, S. Huang, I. Spanopoulos, X. Li, Y. Wang, L. Chen, G. Yang, M. G. Kanatzidis, *ACS Appl. Mater. Interfaces* **2020**, 12, 43885.
- [28] S. Paek, S. B. Khan, M. Franckevičius, R. Gegevičius, O. A. Syzgantseva, M. A. Syzgantseva, S. Kinche, A. M. Asiri, C. Roldán-Carmona, M. K. Nazeeruddin, *J. Mater. Chem. A* **2021**, 9, 5374.
- [29] S. Wu, Z. Li, J. Zhang, T. Liu, Z. Zhu, A. K. Y. Jen, *Chem. Commun.* **2019**, 55, 4315.
- [30] A. D. Jodlowski, A. Yépez, R. Luque, L. Camacho, G. de Miguel, *Angew. Chem., Int. Ed.* **2016**, 55, 14972.
- [31] H. Tan, A. Jain, O. Voznyy, X. Lan, F. P. G. De Arquer, J. Z. Fan, R. Quintero-Bermudez, M. Yuan, B. Zhang, Y. Zhao, F. Fan, P. Li, L. N. Quan, Y. Zhao, Z. H. Lu, Z. Yang, S. Hoogland, E. H. Sargent, *Science* **2017**, 355, 722.
- [32] B. Hwang, Y. Park, J. S. Lee, *J. Mater. Chem. C* **2021**, 9, 110.
- [33] Q. Lin, A. Armin, R. C. R. Nagiri, P. L. Burn, P. Meredith, *Nat. Photonics* **2015**, 9, 106.
- [34] V. Adinolfi, M. Yuan, R. Comin, E. S. Thibau, D. Shi, M. I. Saidaminov, P. Kanjanaboos, D. Kopilovic, S. Hoogland, Z. H. Lu, O. M. Bakr, E. H. Sargent, *Adv. Mater.* **2016**, 28, 3406.
- [35] J. Yao, H. Wang, P. Wang, R. S. Gurney, A. Intaniwet, P. Ruankham, S. Choopun, D. Liu, T. Wang, *Mater. Chem. Front.* **2019**, 3, 1357.
- [36] M. I. Saidaminov, A. L. Abdelhady, B. Murali, E. Alarousu, V. M. Burlakov, W. Peng, I. Dursun, L. Wang, Y. He, G. MacUlan, A. Goriely, T. Wu, O. F. Mohammed, O. M. Bakr, *Nat. Commun.* **2015**, 6, 1.
- [37] B. Murali, E. Yengel, C. Yang, W. Peng, E. Alarousu, O. M. Bakr, O. F. Mohammed, *ACS Energy Lett.* **2017**, 2, 846.
- [38] W. Shi, H. Ye, *J. Phys. Chem. Lett.* **2021**, 12, 4052.
- [39] S. Ryu, J. H. Noh, N. J. Jeon, Y. Chan Kim, W. S. Yang, J. Seo, S. Il Seok, *Energy Environ. Sci.* **2014**, 7, 2614.
- [40] K. Domanski, J. P. Correa-Baena, N. Mine, M. K. Nazeeruddin, A. Abate, M. Saliba, W. Tress, A. Hagfeldt, M. Grätzel, *ACS Nano* **2016**, 10, 6306.
- [41] J. Idígoras, F. J. Aparicio, L. Contreras-Bernal, S. Ramos-Terrón, M. Alcaire, J. R. Sánchez-Valencia, A. Borrás, Á. Barranco, J. A. Anta, *ACS Appl. Mater. Interfaces* **2018**, 10, 11587.
- [42] L. Contreras-Bernal, C. Aranda, M. Valles-Pelarda, T. T. Ngo, S. Ramos-Terrón, J. J. Gallardo, J. Navas, A. Guerrero, I. Mora-Seró, J. Idígoras, J. A. Anta, *J. Phys. Chem. C* **2018**, 122, 5341.
- [43] L. Contreras-Bernal, S. Ramos-Terrón, A. Riquelme, P. P. Boix, J. Idígoras, I. Mora-Seró, J. A. Anta, *J. Mater. Chem. A* **2019**, 7, 12191.
- [44] D. Yang, X. Zhang, K. Wang, C. Wu, R. Yang, Y. Hou, Y. Jiang, S. Liu, S. Priya, *Nano Lett.* **2019**, 19, 3313.